SUPPLEMENTAL FIGURES

Global co-transcriptional splicing in *Arabidopsis* and the correlation with splicing regulation in mature RNAs

Shaofang Li[a,b,1,*], Yuan Wang[c,d,e1], Yonghui Zhao[c,f], Xinjie Zhao[a,b], Xuemei Chen[c], Zhizhong Gong[a,b]

Summary

Supplemental Figure 1. **Clustering analysis of transcriptomes built in this study.**
Supplemental Figure 2. Performance of PI_Junction and PI_Density.
Supplemental Figure 3. Boxplots showing distribution of PI of constitutive and alternative introns.
Supplemental Figure 4. Correlations of intron-surrounding features with PI.
Supplemental Figure 5. **Distribution of PI in chromatin RNAs, total intron number, and gene length for the three groupings**.
Supplemental Figure 6. Total intron number leads to correlations of length of introns and flanking exons with PI in chromatin RNAs.
Supplemental Figure 7. Inefficient co-transcriptional splicing of ncRNAs is not caused by low total intron number.
Supplemental Figure 8. PI distribution in *trans*-acting protein mutants.
Supplemental Figure 9. DSIs in mature RNAs correlate with PI in chromatin RNAs.
Supplemental Figure 10. Comparable splicing efficiency in wild-type transcriptomes.

Figure. S1

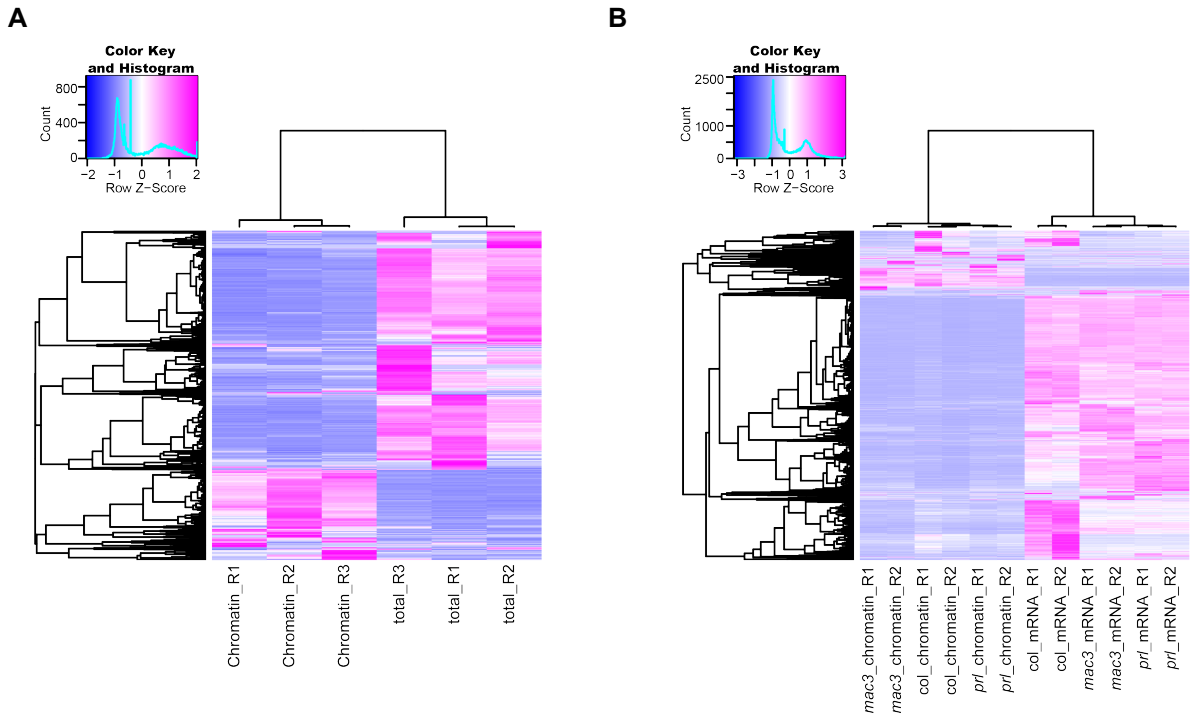

Supplemental Figure 1. Clustering analysis of transcriptomes built in this study.

(A) Heatmap showing the clustering analysis of three replicates of chromatin RNA-seq and total RNA-seq in Col-0. **(B)** Heatmap showing the clustering analysis of two replicates of chromatin RNA-seq and mRNA-seq in Col-0 (col), *mac3a mac3b* (*mac3*), and *prl1 prl2* (*prl*). The 5000 top-varying transcripts were used for the analysis and were grouped based on the correlation distance. R1, R2, and R3 denote three biological replicates.

Figure. S2

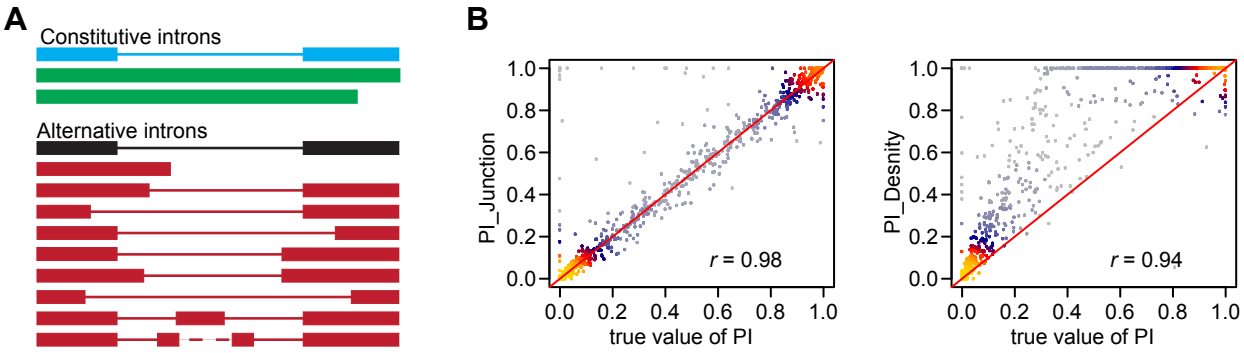

Supplemental Figure 2. Performance of PI_Junction and PI_Density.

(A) Diagram showing constitutive and alternative introns. Rectangles represent exons, lines represent introns, and the dashed line represents the presence of zero or more exons. The blue diagram represents transcripts with constitutive introns that overlap with transcripts shown in green. The black diagram represents transcripts with alternative introns that overlap with one or more transcripts shown in red. **(B)** PI_Junction and PI_Density were calculated on RNA-seq data simulated using Flux Simulator with a known PI. Scatter plots showing the pairwise comparison of PI_Junction and PI_Density with known true value of PI of constitutive introns. Pearson correlation coefficients (*r*) are shown at the bottom right of the plots.

Figure. S3

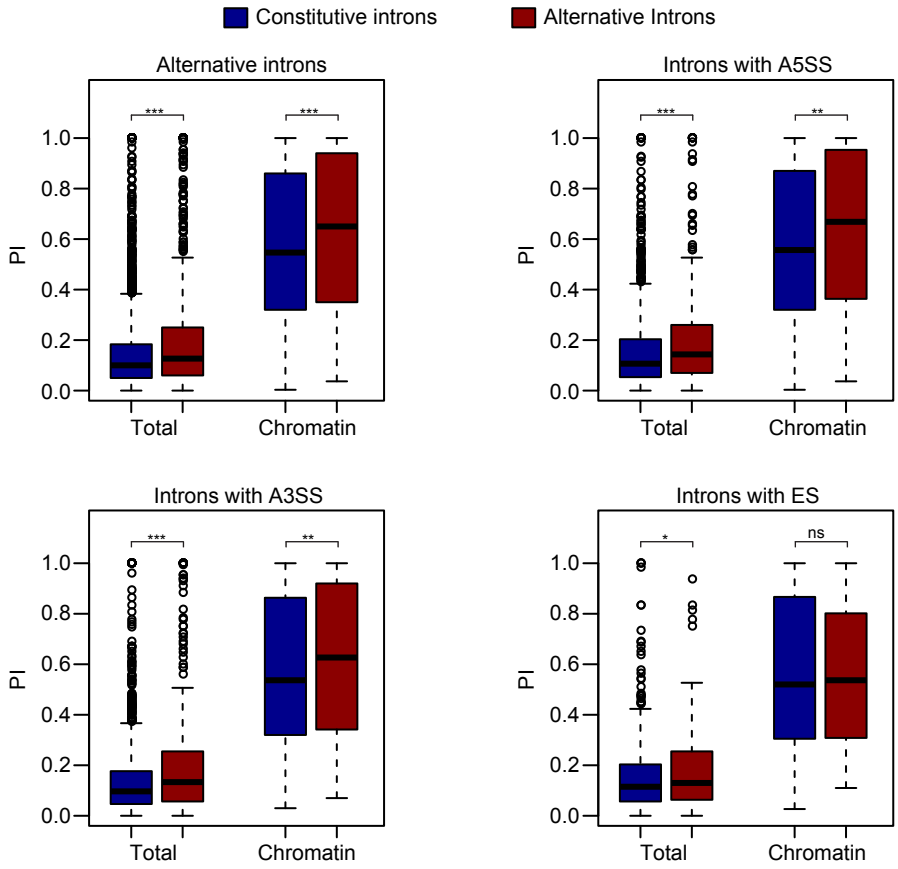

Supplemental Figure 3. Boxplots showing distribution of PI of constitutive and alternative introns.

Boxplots showing PI distribution of constitutive and alternative introns. The plots show all alternative introns as well as introns with A5SS, A3SS, and ES separately. Unlike in Figure 3C, introns in genes with both constitutive and alternative introns were included. ns, $p > 0.1$; *, $p < 0.1$; **, $p < 0.01$; ***, $p < 0.001$ (one-tailed Wilcoxon test).

Figure. S4

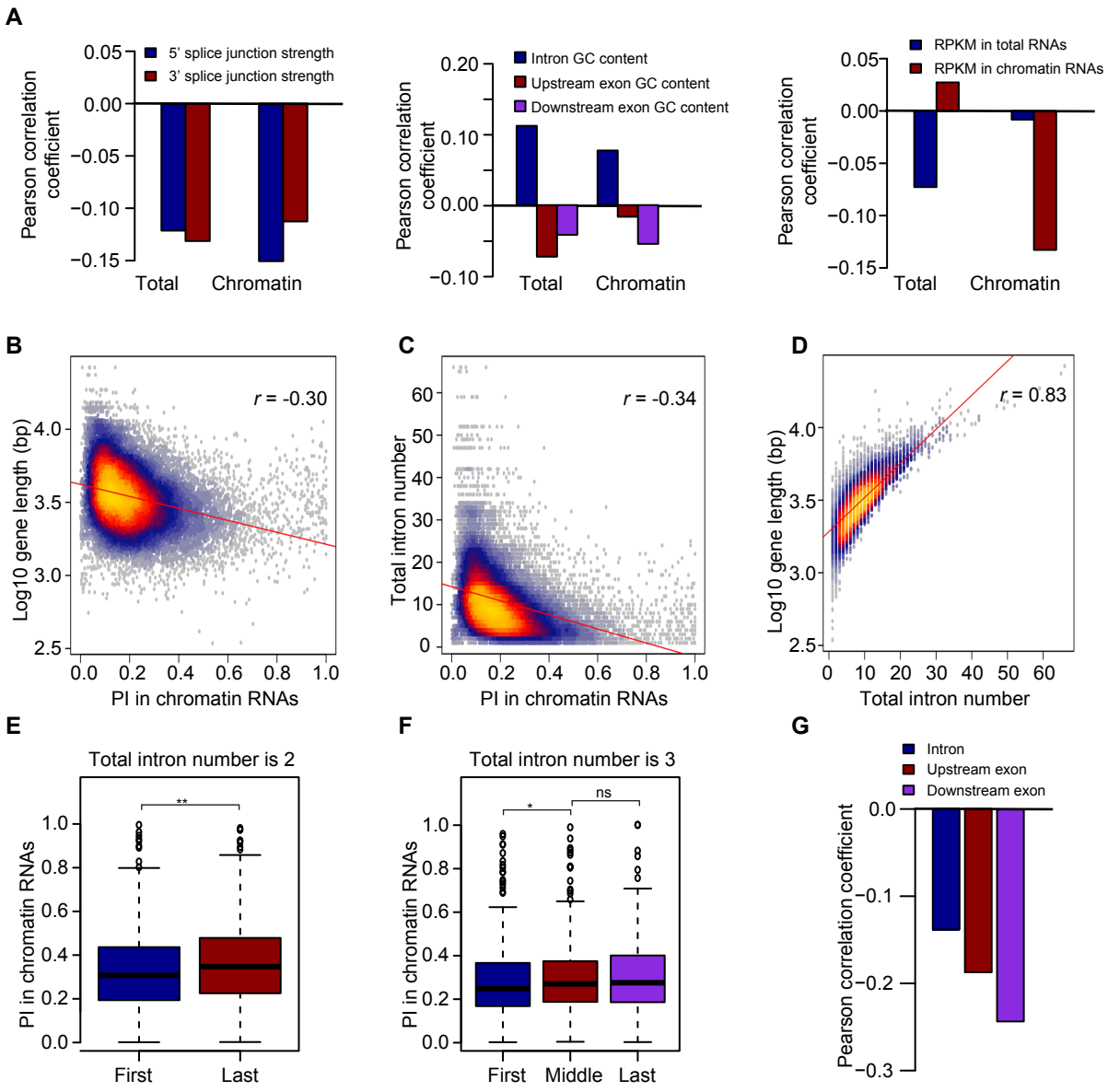

Supplemental Figure 4. Correlations of intron-surrounding features with PI.

(A) Correlations of PI in total and chromatin RNAs with splice junction strength, GC content of introns and flanking exons, and FPKM in total RNAs and chromatin RNAs. **(B–D)** Heatscatter plots showing the correlations between PI in chromatin RNAs and gene length **(B)**, between PI in chromatin RNAs and total intron number **(C)**, and between gene length and total intron number **(D)**. Red lines are linear regression lines. **(E)** Boxplot of PI in chromatin RNAs in first and last introns of two-intron genes. **(F)** Boxplot of PI in chromatin RNAs in first, middle, and last introns of three-intron genes. **(G)** Correlations of total intron number with length of introns, upstream exons, and downstream exons. ns, $p > 0.1$; *, $p < 0.1$; **, $p < 0.01$ (one-tailed Wilcoxon test).

Figure. S5

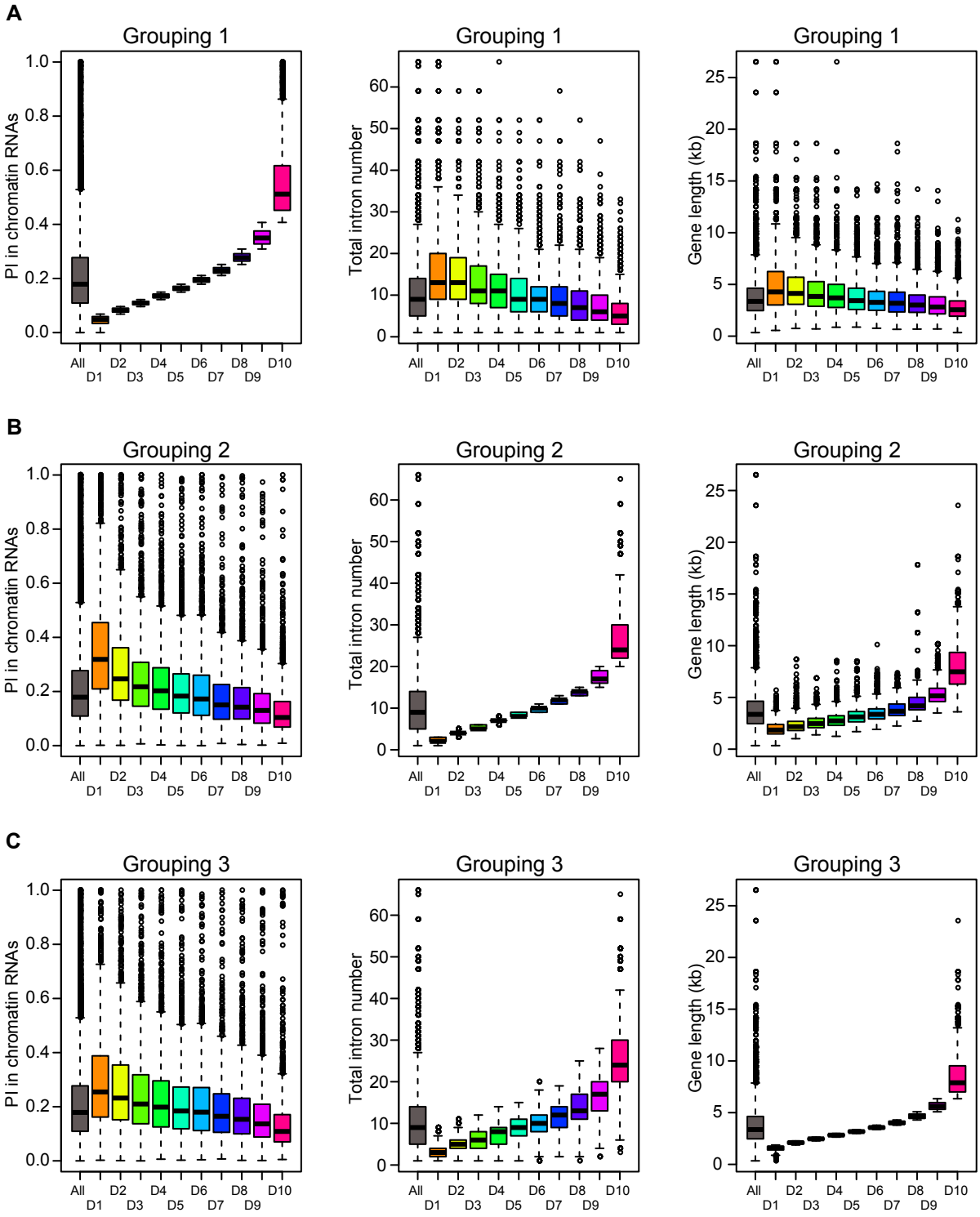

Supplemental Figure 5. Distribution of PI in chromatin RNAs, total intron number, and gene length for the three groupings.

Grouping 1 **(A)**, grouping 2 **(B)**, and grouping 3 **(C)** correspond to the same groupings in Figure 4B.

Figure. S6

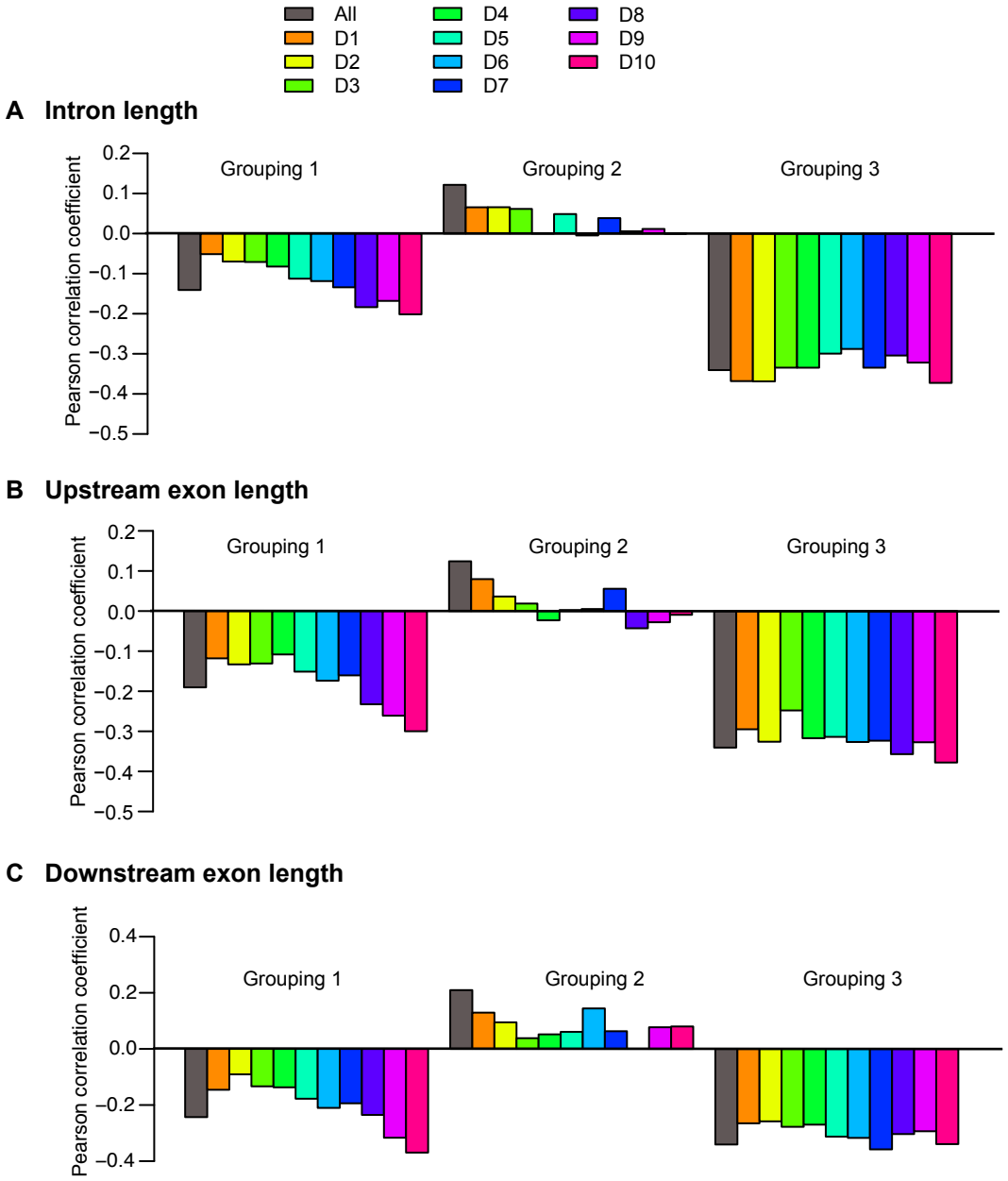

Supplemental Figure 6. Total intron number leads to correlations of length of introns and flanking exons with PI in chromatin RNAs.

Pearson correlations were calculated for three groupings of introns in a similar way as in Figure 4B. In grouping 1, introns were divided into 10 deciles according to an increasing order of PI in chromatin RNAs. Correlations of total intron number with intron length **(A)** or upstream **(B)** or downstream exon length **(C)** were calculated for all introns and the 10 deciles. In grouping 2, introns were divided into 10 deciles according to an increasing order of total intron number. Correlations of PI in chromatin RNAs with intron length **(A)** or upstream **(B)** or downstream exon length **(C)** were calculated for all introns and the 10 deciles. In grouping 3, introns were divided into 10 deciles according to an increasing order of intron length **(A)** or upstream **(B)** or downstream exon length **(C)**. Correlations of PI in chromatin RNAs and total intron number were calculated for all introns and the 10 deciles.

Figure. S7

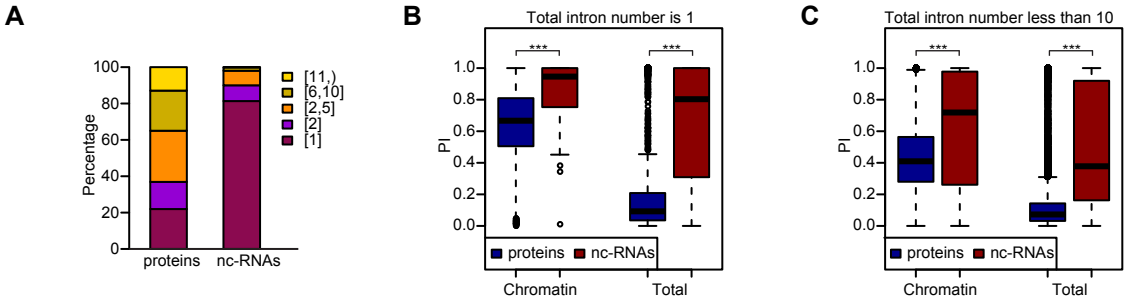

Supplemental Figure 7. Inefficient co-transcriptional splicing of ncRNAs is not caused by low total intron number.

(A) Bar plot showing total intron numbers of proteins and ncRNAs. **(B)** Distribution of PI of introns in single-intron proteins and ncRNAs. **(C)** Distribution of PI of introns in proteins and ncRNAs with total intron number < 10. ***, $p < 0.001$ (one-tailed Wilcoxon test).

Figure. S8

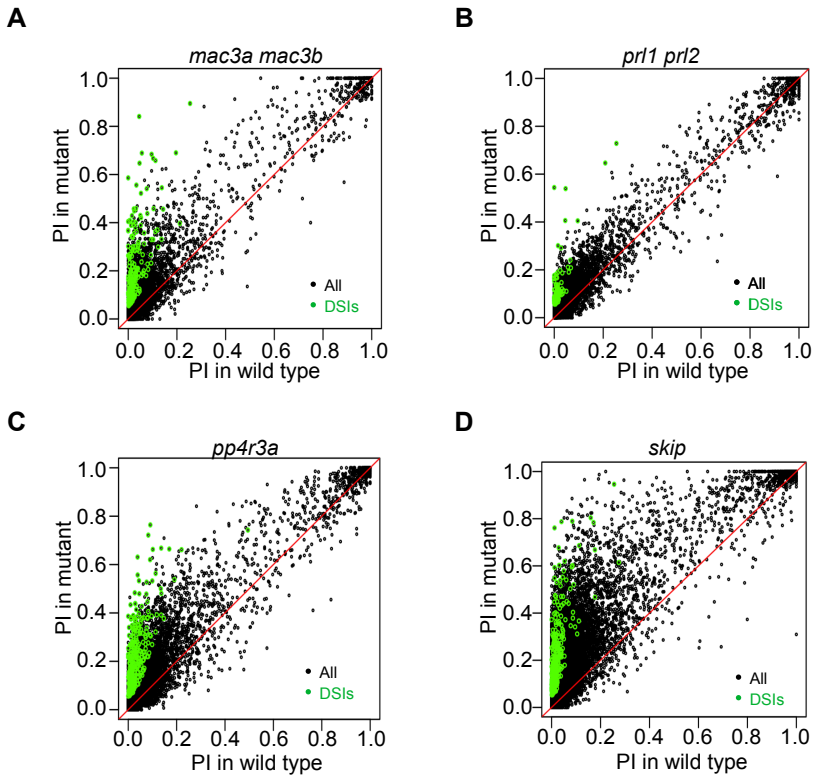

Supplemental Figure 8. PI distribution in *trans*-acting protein mutants.

Scatterplots showing the PI distribution in wild type, *mac3a mac3b* **(A)**, *prl1 prl2* **(B)**, *pp4r3a* **(C)**, and *skip* **(D)**.

Figure. S9

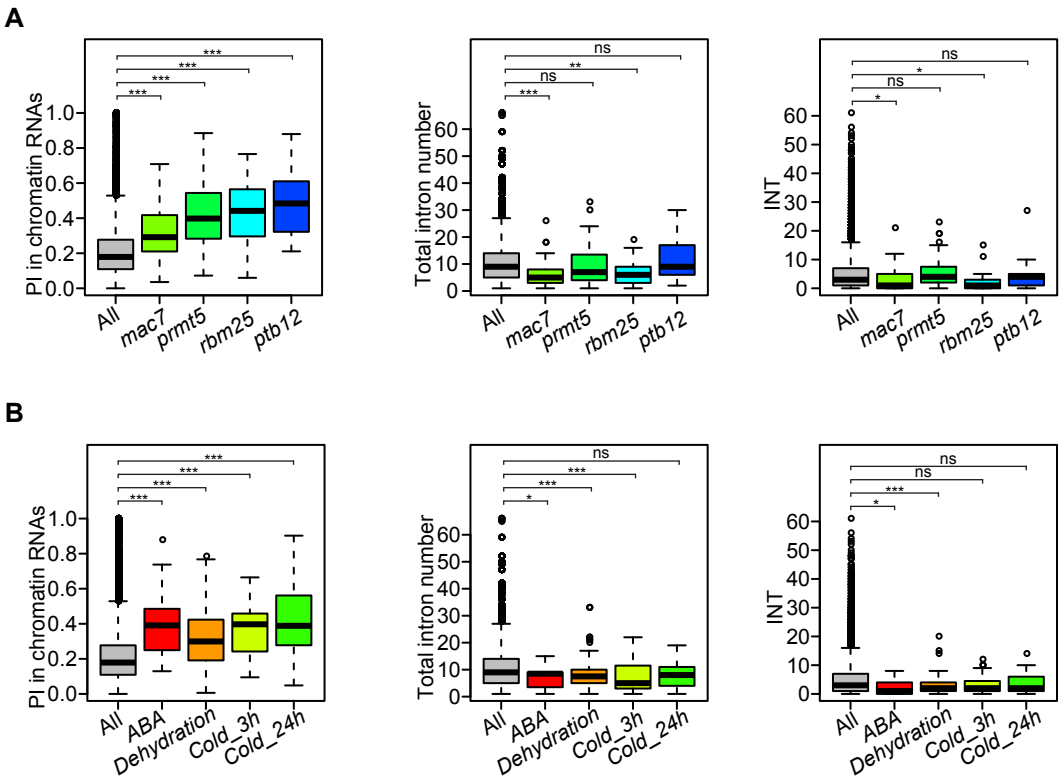

Supplemental Figure 9. DSIs in mature RNAs correlate with PI in chromatin RNAs.

(A) Boxplot showing PI in chromatin RNAs, total intron number, and INT of DSIs regulated in *mac7*, *prmt5*, *rbm25*, and *ptb12*. **(B)** Boxplot showing PI in chromatin RNAs, total intron number, and INT of DSIs upon treatment with ABA, dehydration, and cold. ns $p > 0.1$; *, $p < 0.1$; **, $p < 0.01$; ***, $p < 0.001$ (one-tailed Wilcoxon test).

Figure. S10

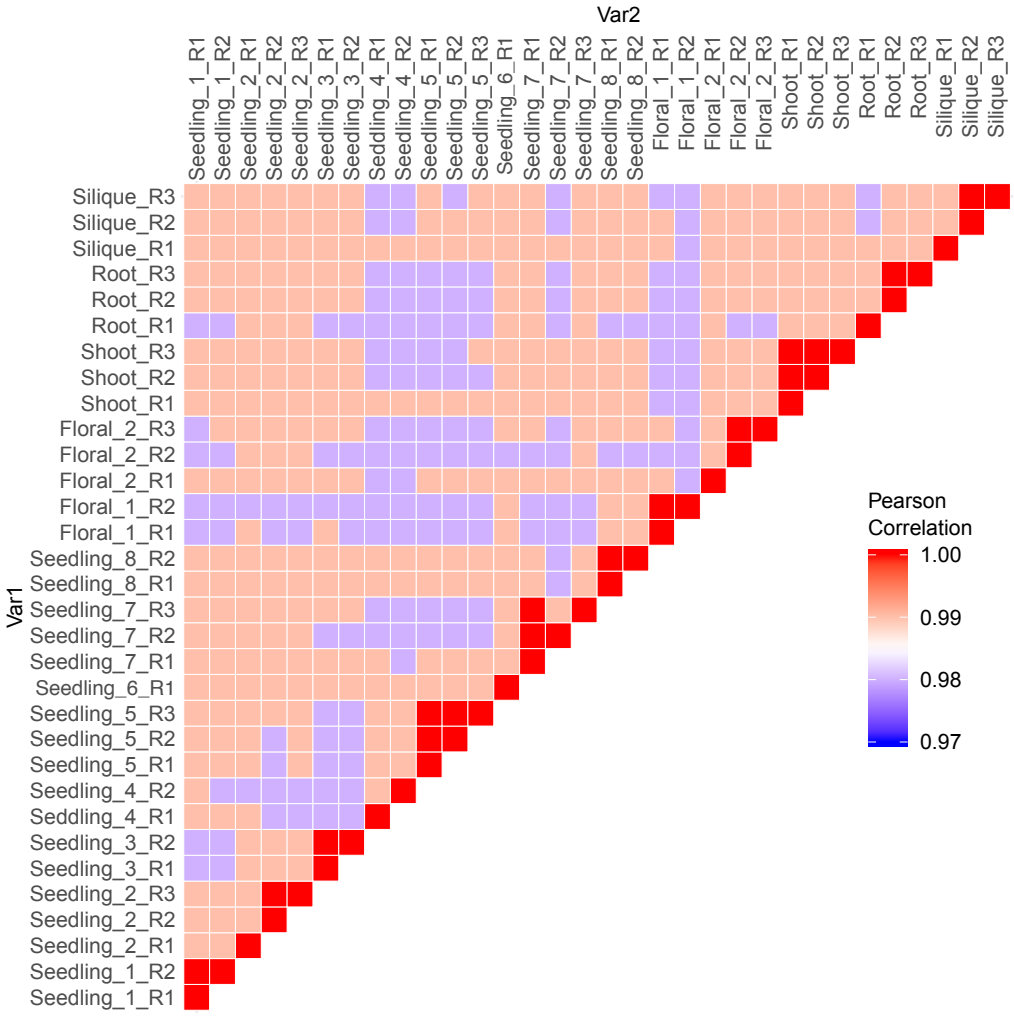

Supplemental Figure 10. Comparable splicing efficiency in wild-type transcriptomes.

Heatmap showing the pairwise Pearson correlation coefficients of PI at constitutive introns calculated from each wild-type mRNA-seq generated in this study (Foral_1_R1 and Floral_1_R2) and from public transcriptomes listed in Supplemental Table 4.